



Supplement of

The improved comparative reactivity method (ICRM): measurements of OH reactivity under high-NO_x conditions in ambient air

Wenjie Wang et al.

Correspondence to: Bin Yuan (byuan@jnu.edu.cn)

The copyright of individual parts of the supplement might differ from the article licence.

22 1. Calculation of X_R

23 Due to the variation of reagent ion source and sample humidity, the pyrrole
24 (C_4H_5N) ion signal is normalized to a standard reagent ion signal of 10^6 counts/s (cps)
25 as following in Eq. 1.

$$26 \quad Pyrrole_{ncps} = \frac{i[C_4H_5NH^+] \times 10^6}{i[H_3O^+] + X_R \times i[H_3O^+H_2O]} \quad (1)$$

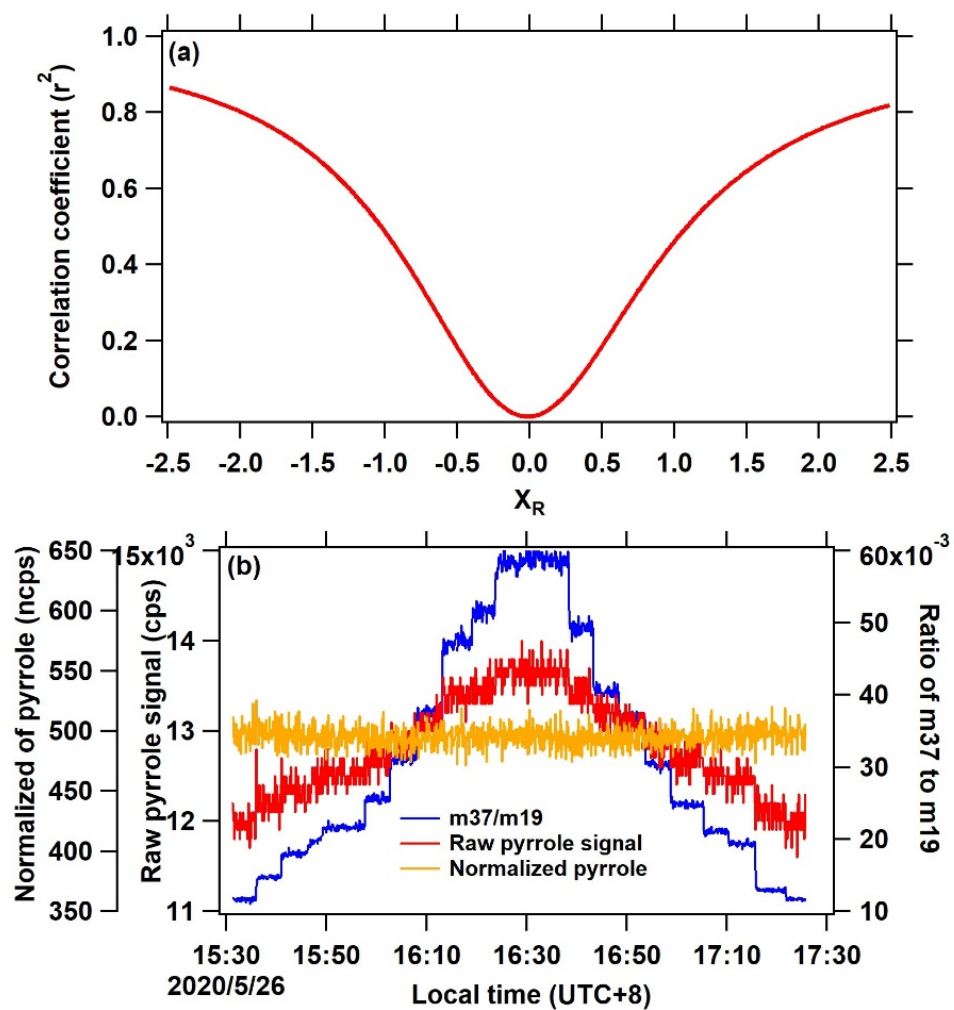
27 Where $Pyrrole_{ncps}$ is a normalized signal of the pyrrole, and $i[C_4H_5NH^+]$,
28 $i[H_3O^+]$, and $i[H_3O^+H_2O]$ represent the signals of different product ions, respectively.
29 The value of X_R not only represents difference in detection efficiencies of detector, but
30 also the difference in rate coefficients of the proton transfer reactions $H_3O^+ + \text{pyrrole}$
31 and $H_3O^+(H_2O) + \text{pyrrole}$ (de Gouw et al., 2003; de Gouw et al., 2007).

32 Here, the X_R value of pyrrole was determined by the laboratory experiment. The
33 $i[C_4H_5NH^+]$, $i[H_3O^+]$, and $i[H_3O^+H_2O]$ were measured from a dry (0%) to 100%
34 humidified pyrrole standard gas, respectively. The pyrrole signal become independent
35 of relative humidity when normalized to $i[H_3O^+] + X_R \times i[H_3O^+H_2O]$. In other
36 words, the correlation coefficient (r^2) of relative humidity and normalized pyrrole signal
37 reaches a minimum at the optimized X_R value. This method is inspired by the
38 calculation of enhancement ratios and the source contribution of different species in the
39 previous studies (Millet et al., 2005; Yuan et al., 2010). Figure S1 (a) shows the result
40 of the correlation coefficient of at different X_R with a bin of 0.01 values. We found that
41 r^2 is the smallest when the X_R value is 0. Figure S1 (b) shows the time series of pyrrole
42 signals before and after normalizing to $i[H_3O^+] + X_R \times i[H_3O^+H_2O]$, respectively. It
43 is shown that pyrrole signal reaches a stable level after normalized with the increase of
44 relative humidity. Therefore, the X_R value is determined as 0.

45

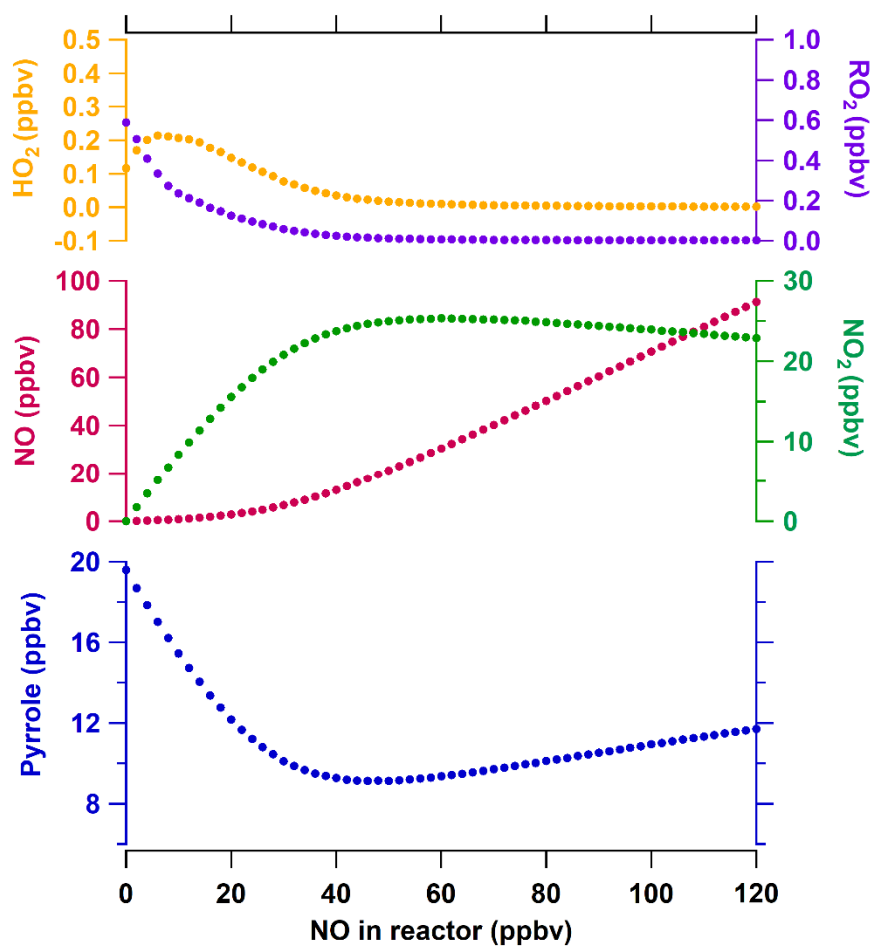
Table S1. The list of all species used to calculate OH reactivity in this study.

Species name	Species name	Species name
Alkanes	n-Undecane	1,2,3-Trimethylbenzene
Ethane	n-Dodecane	p-Diethylbenzene
Propane	Alkenes	m-Diethylbenzene
iso-Butane	Ethene	Alkyne
n-Butane	Propene	Acetylene
iso-Pentane	cis-2-Butene	OVOCs
n-Pentane	trans-2-Butene	Formaldehyde
Cyclopentane	1-Butene	Methanol
2-Methylpentane	1-Pentene	Acetaldehyde
n-Hexane	Isoprene	Ethanol
Cyclohexane	cis-2-Pentene	Acrolein
2,2-Dimethylbutane	trans-2-Pentene	Acetone
2,3-Dimethylbutane	1-Hexene	Furan
3-Methylpentane	Aromatics	MVK+MACR
3-Methylhexane	Benzene	MEK
2,2,4-Trimethylpentane	Toluene	Pentanones
Methylcyclopentane	Ethylbenzene	Phenol
n-Heptane	x, p-Xylene	Furfural
Methylcyclohexane	Styrene	Cresol
2,3,4-Trimethylpentane	o-Xylene	Inorganics
2-Methylheptane	n-Propylbenzene	CO
3-Methylheptane	isopropylbenzene	NO
2,4-Dimethylpentane	o-Ethyltoluene	NO ₂
2,3-Dimethylpentane	m-Ethyltoluene	SO ₂
2-Methylhexane	p-Ethyltoluene	O ₃
n-Octane	1,2,4-Trimethylbenzene	
n-Decane	1,3,5-Trimethylbenzene	



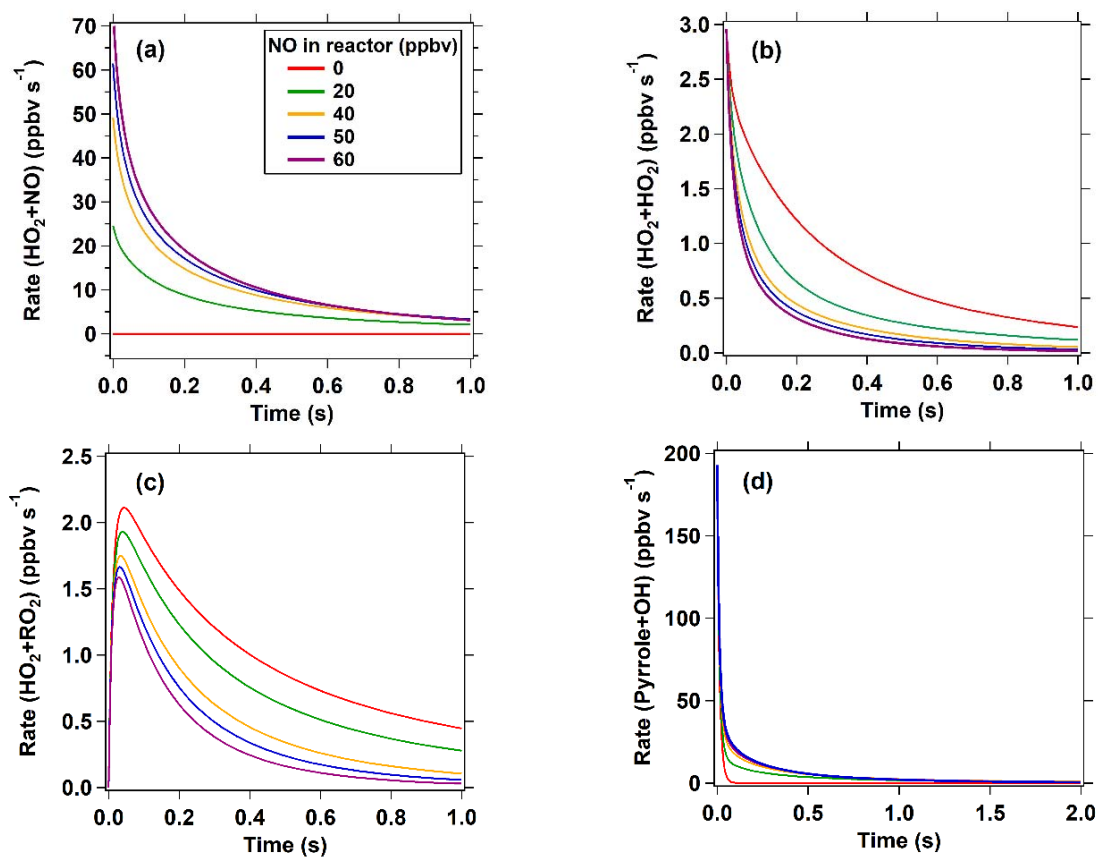
48

49 **Figure S1.** (a) The horizontal represents different X_R values (from -2.5 to 2.5). The
 50 vertical represents the correlation coefficient that pyrrole is normalized to H_3O^+ signals
 51 and m37/m19 at different X_R values. (b) The time series of the signal of pyrrole in cps
 52 (red) and in ncps (yellow, normalized to m19 and m37) with the change of humidity
 53 (blue, represented as the ratio of m37 to m19).



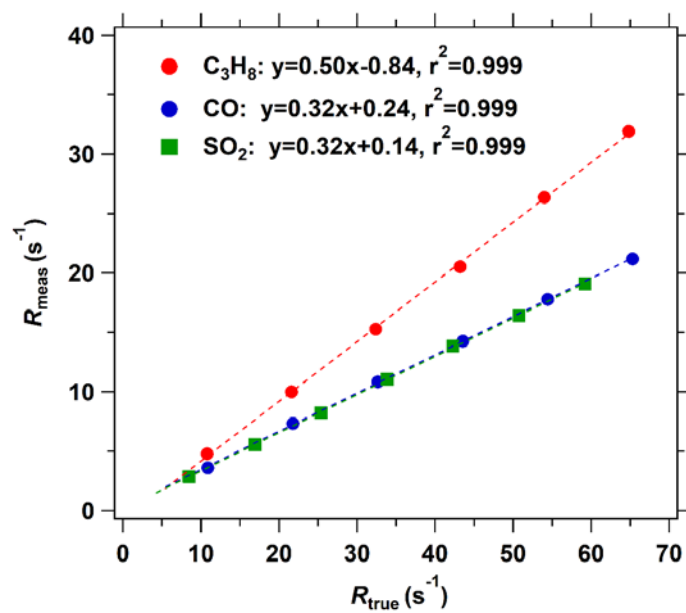
54

55 **Figure S2.** The remaining concentrations of pyrrole, NO, NO₂, HO₂, and RO₂
 56 outflowing of the reactor (with the reaction time of ~ 11 s) as a function of introduced
 57 NO in the reactor.



58

59 **Figure S3.** The reaction rates of HO_2+NO , HO_2+HO_2 , HO_2+RO_2 and $\text{Pyrrole}+\text{OH}$ as a
60 function of reaction time in the reactor. Four levels of introduced NO concentrations (0,
61 20, 40, 50, 60 ppbv) was selected. The reaction time ranging from 0 to 1s is displayed
62 due to the high reaction rates mainly occurred during this period.

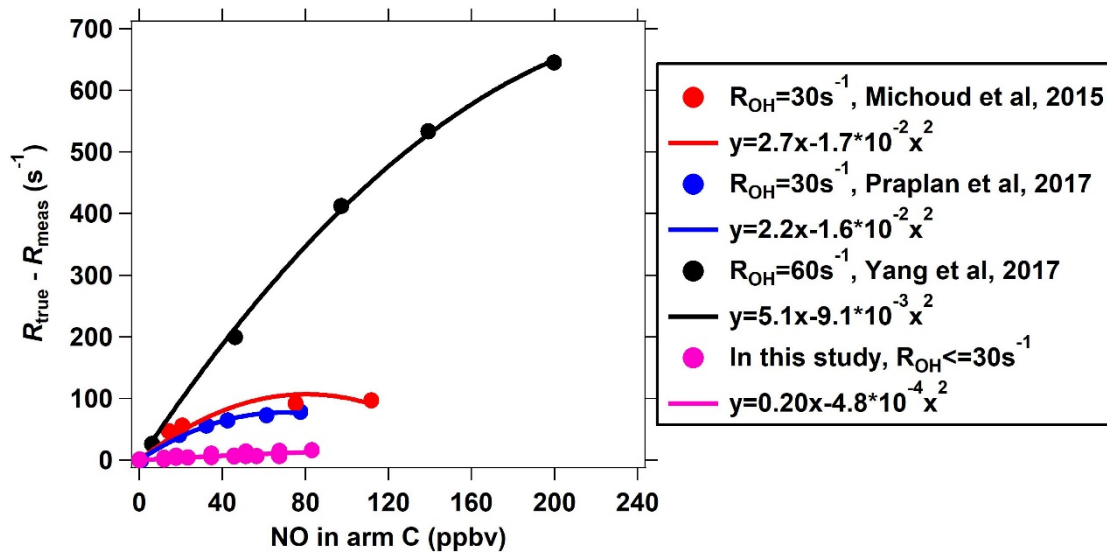


63

64 **Figure S4.** Linear correlation between measured and true OH reactivity of propane,

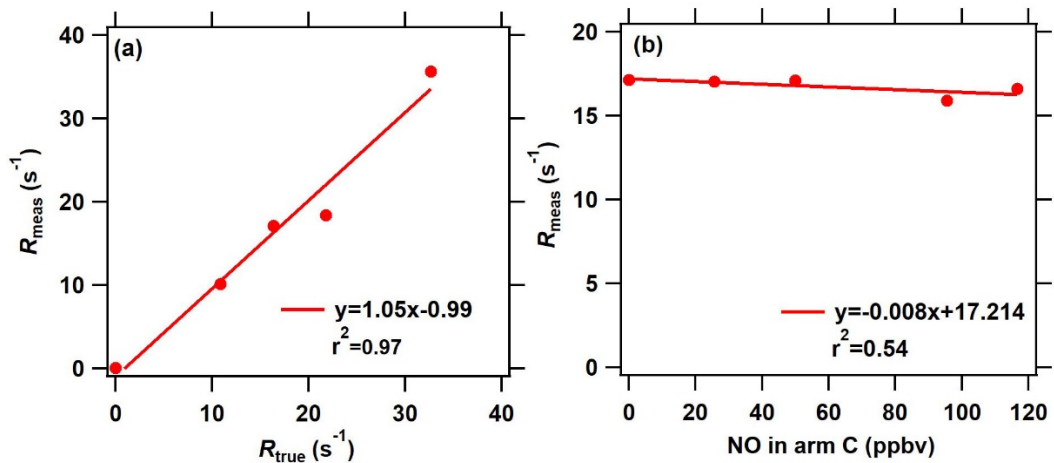
65

CO, and SO₂ simulated by box-model.



66

67 **Figure S5.** The effect of NO on the difference between true reactivity and measured
 68 OH reactivity ($R_{\text{true}} - R_{\text{meas}}$) in the original CRM system. In this study, to correct the
 69 systematic deviation at ambient $\text{NO}=0$, the $R_{\text{true}} - R_{\text{meas}}$ is defined as the difference
 70 between true OH reactivity (R_{true}) and the corrected measured OH reactivity (R'_{meas})
 71 using the calibration factor α_1 ($R'_{\text{meas}} = (\frac{1}{\alpha_1} * R_{\text{meas}})$).

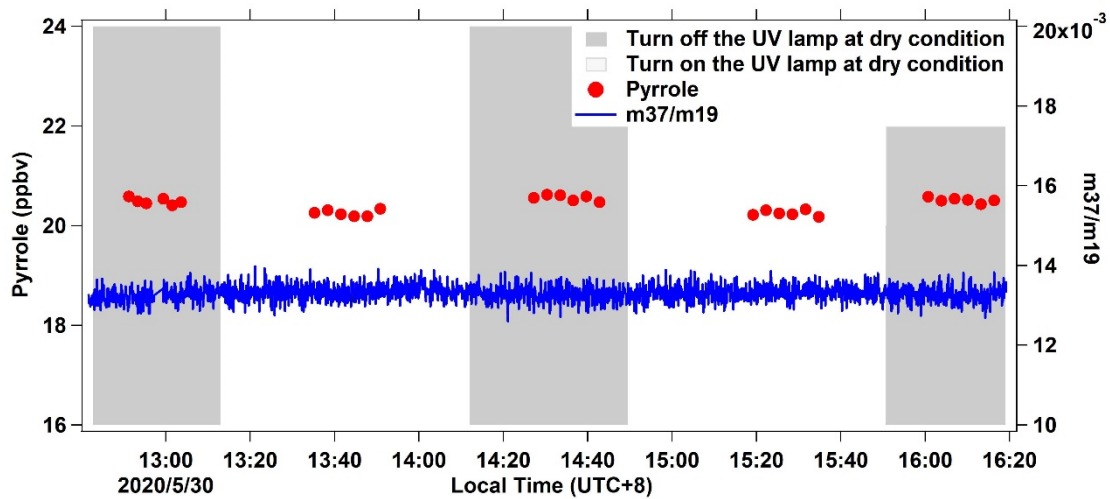


72

73 **Figure S6. (a)** The OH reactivity calibration of NO_2 , **(b)** Comparison of measured and

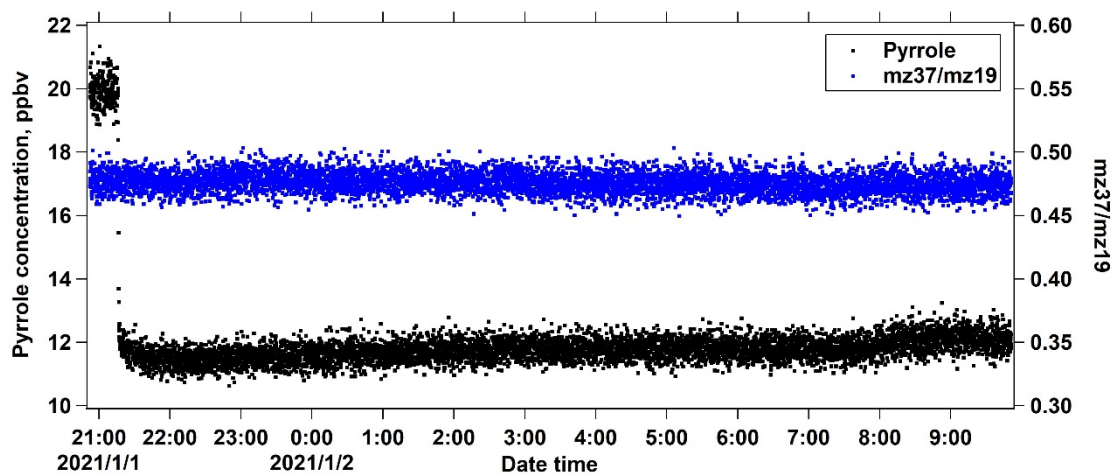
74 true OH reactivity of NO_2 at different NO concentrations introduced through arm C in

75 ICRM system.



76

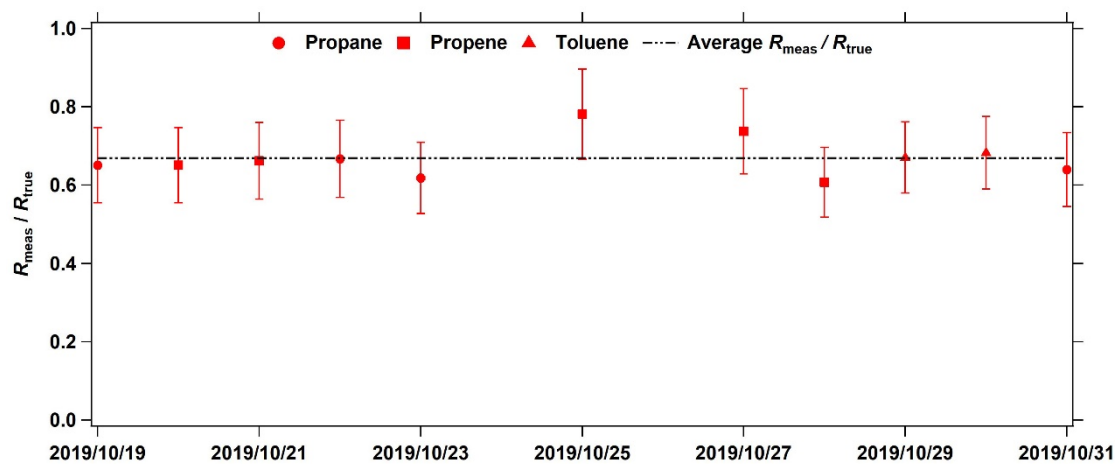
77 **Figure S7.** The variation in pyrrole concentration due to photolysis effect in the ICRM
 78 system. Two modes were tested by turning on and off the mercury lamp at dry condition
 79 (no humidification).



80

81

Figure S8. Total OH reactivity detection limit measured for the ICRM.



82

83 **Figure S9.** The daily calibration of measured reactivity during the field campaign at
 84 Heshan site. The ratio of R_{meas} to R_{true} ($R_{\text{meas}}/R_{\text{true}}$) of each day is given. The dashed line
 85 represents the average value of $R_{\text{meas}}/R_{\text{true}}$ during the measurement. Three VOC standard
 86 gases (propane, propene and Toluene) were used for the calibration.

87 **References**

88 de Gouw, J. and Warneke, C.: Measurements of volatile organic compounds in the earth's atmosphere
89 using proton-transfer-reaction mass spectrometry, *Mass Spectrom Rev*, 26, 223-257, 2007.

90 de Gouw, J. A., Goldan, P. D., Warneke, C., Kuster, W. C., Roberts, J. M., Marchewka, M., Bertman, S.
91 B., Pszenny, A. A. P., and Keene, W. C.: Validation of proton transfer reaction-mass spectrometry
92 (PTR-MS) measurements of gas-phase organic compounds in the atmosphere during the New
93 England Air Quality Study (NEAQS) in 2002, *Journal of Geophysical Research: Atmospheres*,
94 108, 2003.

95 Millet, D. B. and Neil M. Donahue, S. N. P., Andrea Polidori, Charles O. Stanier, Barbara J. Turpin,
96 Allen H. Goldstein: Atmospheric volatile organic compound measurements during the Pittsburgh
97 Air Quality Study: Results, interpretation, and quantification of primary and secondary
98 contributions, *Journal of Geophysical Research*, 110, 1-17, 2005.

99 Yuan, B., Liu, Y., Shao, M., Lu, S., and Streets, D. G.: Biomass Burning Contributions to Ambient
100 VOCs Species at a Receptor Site in the Pearl River Delta (PRD), China, *Environmental Science &*
101 *Technology*, 44, 4577-4582, 2010.

102